Interpretation of pumping tests in a mixed flow karst system

Jean-Christophe Maréchal,[1] Bernard Ladouche,[1] Nathalie Dörfliger,[1] and Patrick Lachassagne[1]

Received 21 June 2007; revised 28 November 2007; accepted 17 December 2007; published 1 May 2008.

[1] A long-duration pumping test performed in the conduit of a mixed flow karst system (MFKS) is analyzed and interpreted. It constitutes a unique experiment of catchment wide response of a karst system, with drawdowns measured both in the pumped conduit and in the matrix. A modeling approach is proposed for this interpretation. The developed double continuum model consists of two reservoirs - karst conduits and the surrounding carbonate rocks - between which flow exchange is modeled using the superposition principle and the hypothesis of Darcian flow in the matrix considered as an equivalent porous media. The karst conduits are assumed to have an infinite hydraulic conductivity. Model calibration results in a very good match (relative root mean square [rRMS] = 2.3 %) with drawdown measured at the pumping well (karst conduit). It shows that the matrix hydrodynamic parameters (hydraulic conductivity and storativity) have a greater influence on the drawdown than the storage capacity of the conduit network. The accuracy of the model relies mostly on a very good knowledge of both pumping rate and natural discharge at the spring (with and without pumping). This type of approach represents an advance in double continuum modeling of karst systems. It also provides a methodology for the management of water resources from karst aquifers.

Citation: Maréchal, J.-C., B. Ladouche, N. Dörfliger, and P. Lachassagne (2008), Interpretation of pumping tests in a mixed flow karst system, *Water Resour. Res.*, *44*, W05401, doi:10.1029/2007WR006288.

1. Introduction

[2] Various approaches have been proposed to deal with karstification and groundwater flow patterns in karst systems when interpreting pumping tests. They depend on the maturity of karst development in carbonate aquifers.

[3] According to the classification of *Quinlan and Ewers* [1985], for poorly developed karst systems or ''diffuse flow karst systems'' (DFKS), classical pumping test interpretation methods for fractured media [*Maréchal et al.*, 2004] can be used in the absence of organized flow. In this case, the karstification increases the order of magnitude of the determined parameters (e.g., transmissivity and storage coefficient). Where there is localized karstification within a fractured formation, fractured media models can be used when the well is not drilled directly into the karst cavity [*Marsaud*, 1997]. The karst structure plays a role only as a recharge boundary [*Marsaud*, 1997].

[4] At the opposite side of the classification of *Quinlan and Ewers* [1985], the ''conduit flow karst systems'' (CFKS), also called ''maturely karstified aquifers'' [*Quinlan and Ewers*, 1985] or ''free flow aquifers'' [*White*, 1969], are characterized by turbulent and possible free surface flow in large solution conduits [*Thrailkill*, 1988]. The characteristic flow pattern is either dendritic or maze-like and a flow continuum does not exist in all parts of the aquifer, namely in the matrix [*Thrailkill*, 1985]. For this type of karst, *Thrailkill* [1988] proposed a specific approach based on drawdown interval analysis. This method disregards the possible diffuse flow from the matrix to the conduits.

[5] In between these two extreme types of carbonate aquifers, ''mixed flow karst systems'' (MFKS, *Quinlan and Ewers* [1985]) can be conceptualized as dual or triple flow systems comprising localized and often turbulent flow in solution conduits and Darcian flow or diffuse flow in the fractures and in the porous rock [*Atkinson*, 1977]. Although pumping tests carried out in wells intersecting the fractured or porous rock matrix appear to be suitable for estimating the hydrodynamic parameters in this aquifer compartment, those done in wells intercepting the solution conduits are difficult to interpret because the geometry of cave networks and connections to the matrix are very often unknown. Moreover, the way how a MFKS would react to a long-duration pumping test in its conduit network is still unknown and there is no example of such an experiment described in the literature till now. Because of the complexity of flow in MFKS, there are few tools well-suited to interpreting pumping tests in such highly heterogeneous media [*Jones*, 1999]. The approach proposed by *Thrailkill* [1988], which disregards the possible diffuse flow from the matrix to the conduits, can be used only for short-duration (a few hours) pumping tests. It is unsuitable for the long-duration tests in MFKS discussed in this paper. Past attempts to interpret pumping test in MFKS have dealt only with hydrochemical aspects for the evaluation of the renewal of the exploitable water [*Reynaud et al.*, 1999] or with a preliminary interpretation of drawdown [*Bakalowicz et al.*, 1994; *Debieche et al.*, 2002]. The only methodology for a quantitative interpretation has been proposed by *Marsaud*

[1] BRGM (Bureau de Recherches Géologiques et Minières), Water Division, Montpellier, France.

0043-1397/08/2007WR006288$09.00

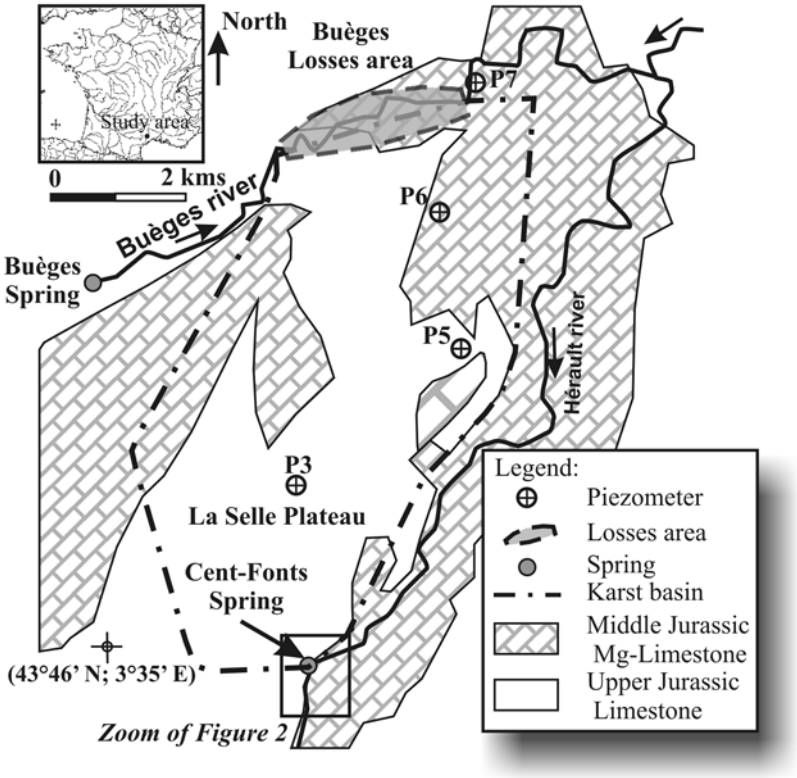

Figure 1. Geological and location map of the Cent-Fonts karst system. A simplified hydrogeological cross-section is given in Figure 7.

[1997]. This approach, limited to the case of a pumping in a well located in the matrix of the system or in the annex drainage systems (large cavities not directly connected to the karst conduits), is based on the interpretation of fluctuations in spring discharge rates during pumping.

[6] The present paper describes a long-duration pumping test performed in a well intersecting the solution conduits of a mixed flow karst system. The response of the system is analyzed into the solution conduit and the surrounding carbonate rocks (matrix). An approach using a double-continuum model is developed for the interpretation of drawdown into both the conduit and the matrix. The model comprises two reservoirs dealing with conduit flow in karst drains and diffuse flow in the matrix. The exchange of flow between the two reservoirs is explicitly modeled using a physically based approach (varying difference in hydraulic heads) through the application of the superposition principle. The method is applied to a real case study, the Cent-Fonts karst system in the Hérault region of Southern France (Figure 1).

2. Study Site and Data

2.1. Cent-Fonts Karst System

[7] The Cent-Fonts karst (Figure 1) is a mixed-flow karst system located north of Montpellier (Hérault region, Southern France) in a thick limestone and dolomite series (Middle and Upper Jurassic). It has been characterized by long-term monitoring (1997–2007) and numerous studies [*Ladouche et al.*, 1999, 2002, 2005, 2006; *Aquilina et al.*, 1999, 2005, 2006].

[8] The Cent-Fonts spring, located on the right bank of the Hérault River, is the only outlet of the karst system (Figure 1). Its discharge ranges from Q_S = 0.220 m^3/s (during severe low water stage periods) to more than 12 m^3/s during peak flow in winter or spring, the average spring discharge having been about 1 m^3/s during the 1997–2005 period [*Ladouche et al.*, 2005]. The Cent-Fonts spring is the outlet of a water-saturated karst conduit network that has been partially explored and mapped by divers [*Vasseur*, 1993] in the vicinity of the spring, particularly for the purpose of the pumping well sitting [*Bardot*, 2001; *Ladouche et al.*, 2005]. The network is developed below the Hérault River to a depth of at least 95 m (Figure 2). In the mapped area, the cross-sectional area of the karst drain ranges from 4 m^2 to 16 m^2 and its largest part (a 400 m^3 cavity) is located at the end of the explored karst conduit (Figure 2). Three wells intercept the karst network near the spring (Figure 2): CGE is about 60 m deep, F3 is located about 100 m upstream from CGE and reaches the largest part of the conduit at a depth of 128 m, and F2 is located 3 meters from F3 in the same conduit. The observation wells located within the karst basin (P3, P5, P6 and P7, Figure 1) do not intersect the conduit network.

[9] The Buèges valley and the Cévennes fault constitute the Northern and Northwestern boundaries of the catchment area of the Cent-Fonts spring, the Hérault valley being the Southeastern boundary. Morphologically, the area is defined as a plateau representing the relicts of an Oligocene paleosurface that was uplifted during the late Tertiary to an elevation of 200 to 500 masl. The plateau, called "Causse de la Selle", is deeply cut by the Hérault River, which flows

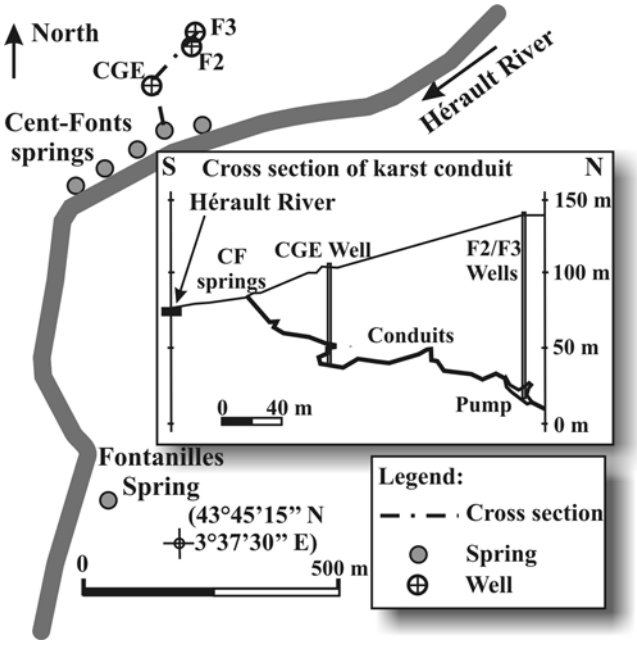

Figure 2. Location of pumping well (F3) and observation wells; cross section showing the wells intersecting the conduit network [*Bardot*, 2001; *Ladouche et al.*, 2005].

at an elevation of about 76 masl near the spring and constitutes the present-day base level of the karst system. Sinkholes in the Buèges River (Figure 1) provide 50 % of the annual mean recharge of the Cent-Fonts karst aquifer system, the rest being diffuse recharge through the epikarst by precipitation on the karst catchment area. The recharge area of the Cent-Fonts system, including the watershed of the sinkhole system, is estimated to be 60 km^2. The area of the sinkhole system is 30 km^2 [*Ladouche et al.*, 2002; *Aquilina et al.*, 2005] and the karst system basin itself has an area A = 30 km^2.

2.2. Pumping Test Data

[10] Pumping tests were done on the Cent-Fonts karst system (well F3) in 2005 along with coupled hydrological and geochemical (major ions, trace elements and Sr isotopes) monitoring. This paper discusses hydrological results only, the study of geochemical results having been presented elsewhere [*Ladouche et al.*, 2007]. The main objectives of the pumping tests were to evaluate the capacity of the tapped conduit to mobilize the reserves of the karst aquifer and to identify the potential impact of the pumping on adjacent groundwater systems, on the underground micro fauna and on the Hérault River.

[11] Step-drawdown tests were done at the end of July 2005 (27 July 2005 to 30 July 2005) during a severe low-water period (low flow hydrologic conditions characterized by a 30-year return-period) with no recharge by rainfall (Figure 3). Four steps with flow rates of 0.2 m^3/s, 0.3 m^3/s, 0.5 m^3/s and 0.4 m^3/s each lasting 6 h with 18 h of recovery, were done in well F3. The non-linear well loss coefficient C has been evaluated to 7 m/(m^3/s)^2 using classical *Jacob* [1947] method. These non-linear head losses generate a theoretical additional drawdown in the well of about 1.2 m at the long-duration pumping rate (0.4 m^3/s). The minor difference in drawdown (17 cm as an average, with no significant variation with time) in the pumping well and in the nearby (3 m) observation well (F2) intersecting the same conduit shows that real well losses are centimeter-size. Therefore the computed non-linear head losses occur in the karst conduit network itself and can thus propagate far away from the pumping well. Hydraulic analysis of flows in conduits shows that the average Reynolds number $R_e = \frac{PD}{S\nu} \approx$ 1.4E05 is superior to the critical value (10000 = $R_{e_{crit}}$) with ν being the kinematic viscosity of water (1.17E-06 m^2/s for water at 14°C), D the mean diameter of the conduits (3.5 m according to speleological measurements, *Vasseur* [1993]), S the mean cross-sectional area of flow (9.8 m^2) and P the pumping rate (0.4 m^3/s). With the lowest pumping rate and the largest cross-sectional area, the Reynolds number is still such that flow is turbulent in the conduit. This confirms that

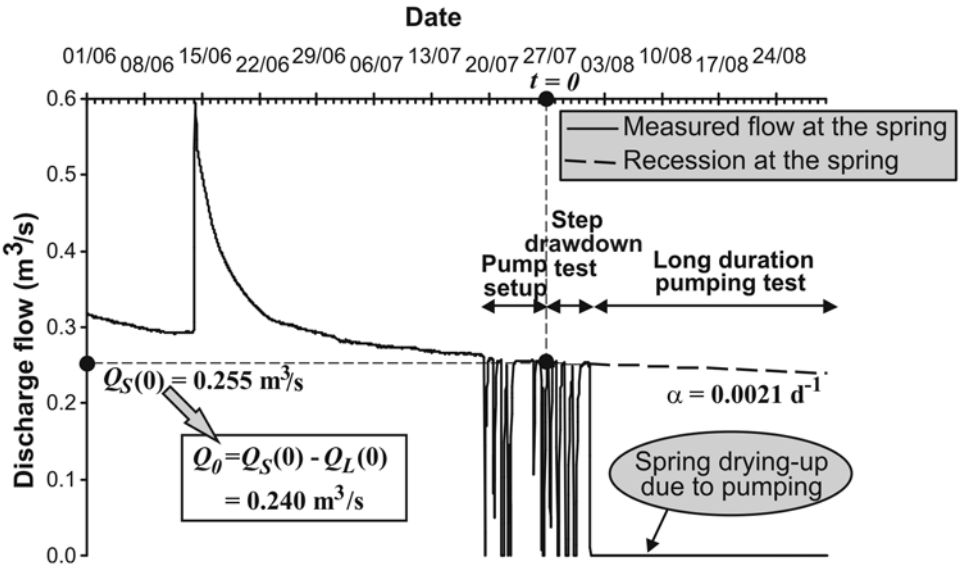

Figure 3. Discharge at the spring before and during the pumping test.

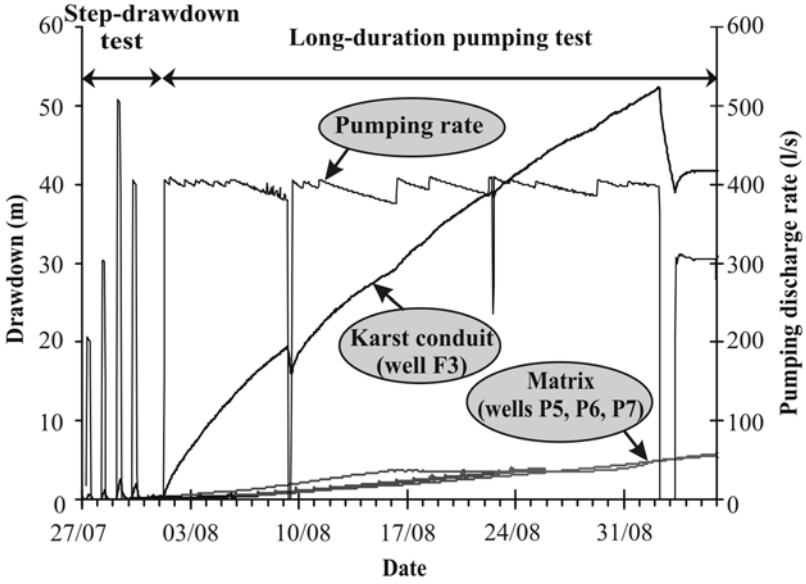

Figure 4. Drawdown during the pumping test. Drawdown is high in the karst conduits (well F3) and low in matrix (P5, P6, and P7). Drawdown at F2 in the karst conduit (not shown here) is very similar (17 cm average difference) to drawdown at F3.

turbulent flow is the cause of the (relatively small) quadratic head losses that occur in the conduit network.

[12] The long duration pumping test began with a 0.4 m^3/s flow rate on 1 August 2005. During this pumping test, which lasted more than one month (1 August 2005–6 September 2005), pumping was halted twice on-purpose (9 August 2005 and 2 August 2005) and stopped once due to electrical problems (22 August 2005 less than one hour) and once due to a storm event at the end (6 September 2005). The heavy rainfall at the beginning of September 2005 induced a peak flow at the spring and consequently temporary stopped the pumping test. For the interpretation, we focus on the 1 August 2005–6 September 2005 period during which there was no external hydrological perturbation of the system.

[13] According to available differential gauging measurements (continuous monitoring) up- and downstream the sinkhole system [*Ladouche et al.*, 2002], the Buèges river losses contribution was constant at $L = 0.015$ m^3/s during the entire test. The mixing theory applied to the chemical characteristics of the pumped water and direct measurements within the dewatered conduit during the pumping test indicate that infiltration of Hérault River water to the conduits occurs only in the immediate vicinity of the spring and reaches $Q_R = 0.030$ m^3/s after 1 August when the hydraulic head in the karst conduit drops below 75 m [*Ladouche et al.*, 2005]. The initial discharge rate at the spring before pumping (27 July 2005) was measured at $Q_S(0) = 0.255$ m^3/s and the recession coefficient at that time was $\alpha = 0.0021$ d^{-1} (Figure 3).

2.3. Drawdown Curves in the Matrix and Karst Conduits

[14] During the test, drawdown was measured at 5 min intervals at F3 (pumping well in the karst conduit) and at P5, P6, and P7 (observation wells located in the matrix according to the interpretation of previous long-term piezometric monitoring [*Ladouche et al.*, 2005]) (Figure 4). In the matrix, the drawdown is low ($s_{m\ \max} \approx 5.1$ m as an average on P5, P6, and P7 at the end of the long-duration pumping test) and depends on the location of the observation wells to karst heterogeneities and on the distance of the piezometers from the pumped conduit network. Measured water level decline in the matrix includes the natural recession of the karst system and is therefore not only induced by the pumping test. On the basis of the average natural water level recession before pumping tests (P5 = 3.6 cm/day, P6 = 9 cm/day, P7 = 8.5 cm/day), the water level decline measured in P5 during the long-duration step is identified as due to both natural recession (25%) and pumping (75%). In P6 and P7, natural recession represents approximately 50% of the measured water level decline. It is also observed that the pumping rate changes do not induce any noticeable change in drawdown curves in the matrix which absorbs short-term fluctuations.

[15] The final drawdown in the karst conduit is high ($s_{c\ \max} = 52.17$ m; Figure 4) and does not show any sign of stabilization after one month of pumping. These results show that both matrix (several kilometers away from the pumping well) and conduits are affected by the test but the matrix is much less affected by pumping than the karst conduit.

[16] Given that the drawdown in the matrix is low, hardly distinguishable from natural recession and dependant on several unknown parameters (conduits geometry, matrix heterogeneities, etc.), the interpretation of the pumping test was focused on the drawdown in the main karst conduit leading to the spring. This approach is coherent with the classical approach in karst hydrology: as a consequence of the high heterogeneity of karst systems, piezometers in the matrix are considered to only provide local information as they are often disconnected from the conduit network and thus not really representative of the functioning of the karst aquifer (*Bakalowicz*, 2005; see also discussion by *Ford and Williams* [1989]).

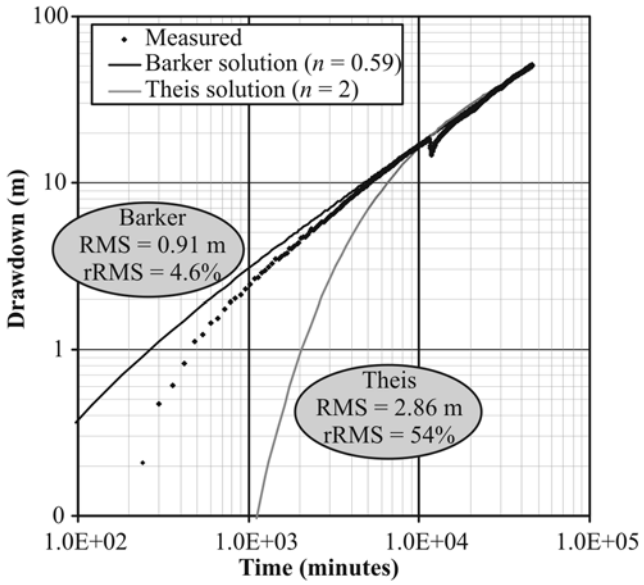

Figure 5. Interpretation of measured drawdown using Theis and Barker analytical solutions.

[17] The difficulty in matching the classical Theis analytical solution (relative root-mean square rRMS = 54 %) on measured drawdown in the karst conduit at the pumping well leads us to consider that the radial model, which assumes that the aquifer is homogeneous, is not well-suited to the present case (Figure 5). The shape of the drawdown curve in the karst conduit (without any long-term stabilization) suggests a non classical flow geometry [*Barker*, 1988]. The generalized radial flow (GRF) approach of Barker could thus be applied [*Walker and Roberts*, 2003] in order to characterize the flow geometry.

[18] The log-log diagnostic plot [*Bourdet et al.*, 1983] of drawdown s and its derivative at the pumping well in the main karst conduit has been analyzed. The common logarithm of drawdown change is plotted versus the common logarithm of elapsed time, together with $\log(ds/d\ln t)$, the common logarithm of the derivative of drawdown change with respect to the natural logarithm of time (Figure 6). There is no evidence of double-porosity type behavior as might have been expected in such a karst system but the presence of two straight line segments. Several authors (*Ehlig-Economides* [1988] and *Walker and Roberts* [2003] among others) noticed that the drawdown derivative displays straight lines at late time, with slopes related to the domain dimensionality and boundary conditions. *Mishra* [1992] showed that the late-time slope of the drawdown derivative for an infinite-acting system is related to the GRF model by:

$$\nu = \lim_{t\to\infty} \frac{d}{d(\log t)}[\log(ds/d\ln t)] \quad (1)$$

and the flow dimension n can be found as $n = 2 - 2\nu$. At early times (Figure 6), the drawdown derivative follows a straight line of unit slope, indicating a period of a few hours during which the storage effects in the karst conduit prevail [*Kruseman and de Ridder*, 1991, p. 273]. This straight line turns into another straight line with a slope $\nu = 0.70$ for late time. This slope corresponds to a flow dimension $n = 0.59$. One-dimensional flow conditions thus tend to prevail in this aquifer.

[19] Measured drawdown corrected from quadratic head losses in the conduits has been matched, using GRF Barker's analytical solution (1988), with the flow-dimension determined here above (Figure 5). The Barker model matches (rRMS = 4.6 %) the measured drawdown better than the Theis analytical solution. Resulting parameters are detailed in Table 1. The considered discharge rate corresponds to the net abstraction by pumping P_N with respect to the initial state: the pumping rate P minus recession flow Q_S at the spring (including inflow from the Buèges river losses) and the Hérault river contribution Q_R:

$$P_N = P - Q_S - Q_R = 0.4 - 0.255 - 0.030 = 0.115\ \mathrm{m^3/s} \quad (2)$$

[20] The value of the hydraulic conductivity K_f (Table 1) has little real physical meaning with respect to the complexity of flow in the karst system: it corresponds to an equivalent characteristic of the system. A modeling approach can only provide physical parameter estimates for the different subsystems of the karst aquifer.

3. Modeling Methodology

[21] Karst water hydraulics is strongly governed by the interaction between a highly conductive conduit network and a low-conductive rock matrix under variable boundary conditions [*Liedl et al.*, 2003]. Figure 7 shows a conceptual model of the Cent-Fonts mixed flow karst system with well F3 intersecting the conduit. The karst system (Figure 7a) comprises a main spring connected to a conduit network recharged by surface water losses in a sinkhole system and by flow from the matrix to the conduits. During the pumping tests (Figure 7b), the highly permeable solution conduits act collectively as the initial source of the water being pumped (see the storage effect of the karst conduits

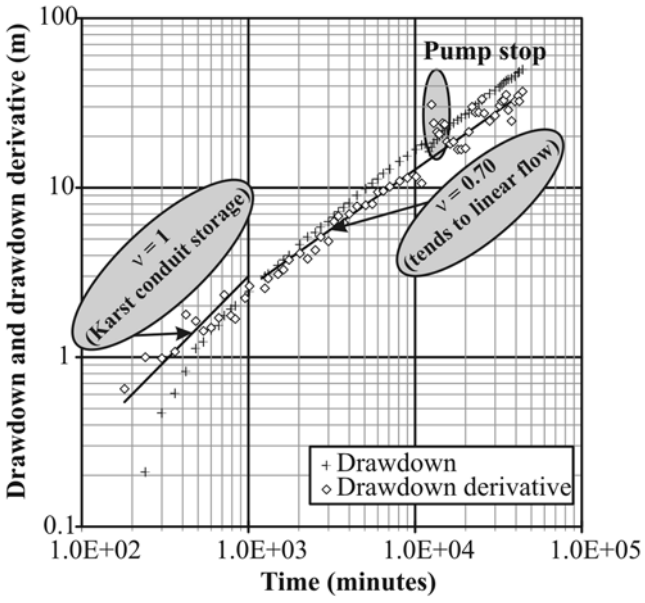

Figure 6. Log-log diagnostic plot of drawdown and drawdown derivative at the pumping well.

Table 1. Calibrated Parameters of Analytical Solutions

Model	Well Characteristics	Symbol	Value	Unit
Radial (Theis)	Pumping discharge rate	P_N	0.115	(m^3/s)
	Well radius	r_w	0.5	(m)
	Global transmissivity	T	3.5E-04	(m^2/s)
GRF (Barker)	Flow dimension	n	0.59	(−)
	Extension of flow	b	50	(m)
	Modified dimension	v	0.705	(−)
	Hydraulic conductivity	K_f	5.0E-06	(m/s)
	Generalized transmissivity	$Kf*b\hat{}(3-n)$	6.2E-02	($m^{3.4}$/s)
Vertical fracture (Ramey and Gringarten)	Matrix transmissivity	T_m	1.2E-05	(m^2/s)
	Matrix storage coefficient	S_m	5.9E-03	(−)
	Storage in well plus vertical fracture	C_{vf}	366	(m^2)

on the diagnostic plot, Figure 6). Consequently, the hydraulic head in the solution conduits decreases (high drawdown in the conduit network), resulting in an increase in the hydraulic gradient between the matrix and karst conduits. This causes water in the fractures and/or in the porosity of the matrix to flow toward the larger solution conduits at a higher rate than before pumping. At the karst basin scale, since the matrix has a much higher storage capacity than the

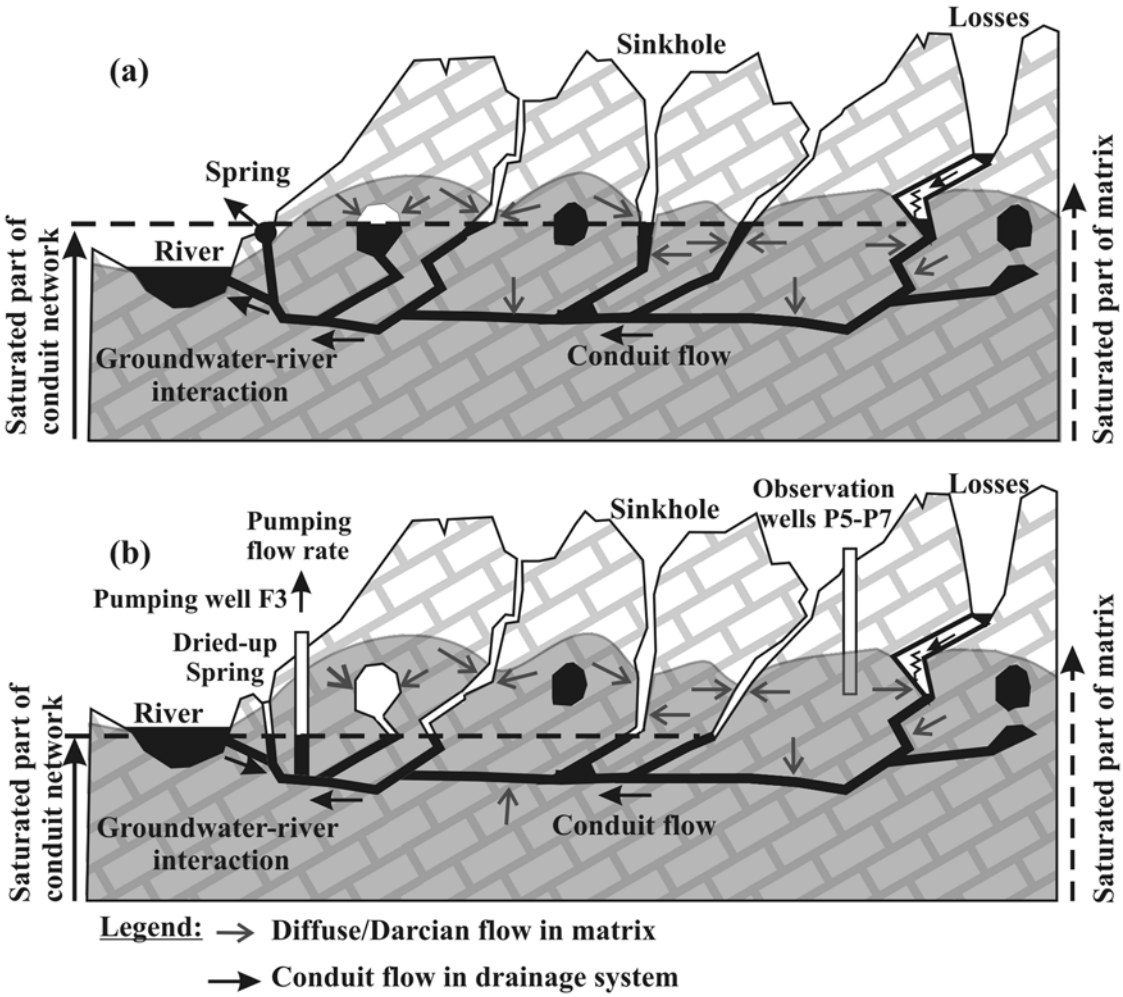

Figure 7. Conceptual model of the Cent-Fonts karst system under natural conditions and during pumping. Mixed flow karst system (a) under natural low flow conditions and (b) when pumping is done in a well intersecting the solution conduit of the same karst system (black: Water in solution voids and conduits; grey: Water in matrix). During pumping, the drawdown is high in the conduits and negligible in the matrix.

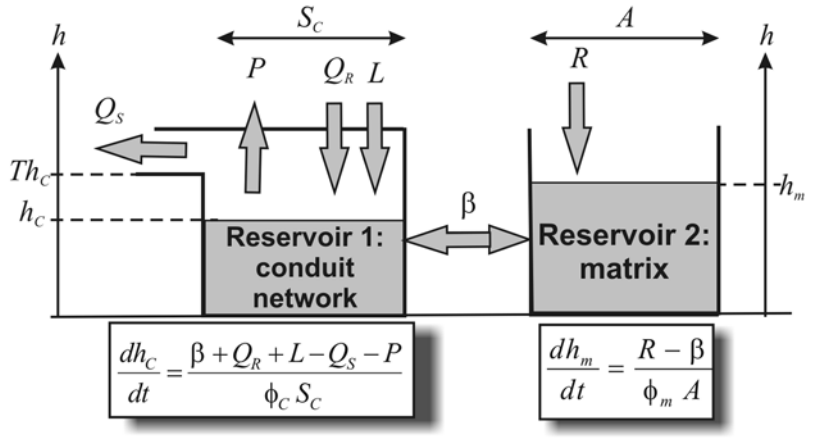

Figure 8. Sketch of the 2 reservoirs: Model and volume conservation equations.

conduits, the hydraulic head fluctuates much less in the matrix than in karst conduits during the pumping test (very low drawdown in the matrix).

3.1. Double Continuum Model

[22] In this type of hydrogeological context, the pumping tests data might represent a measurement of the composite hydraulic response of families of fractures and/or porosity in the matrix and solution conduits [*Streltsova*, 1988]. Therefore to describe the hydraulic properties of the karst aquifer and interpret pumping tests carried out in MFKS, the rate of flow exchange between the matrix and the solution conduits must be identified along with other physical parameters. This constitutes a challenging task because there is no direct way to determine it.

[23] To date, three types of modeling approaches have been used to simulate the hydraulic interaction between the matrix and a conduit network in MFKS [*Teutsch and Sauter*, 1998; *Liedl et al.*, 2003]. In the first approach, multiple sets of fractures were connected to each other in order to represent the hydraulic properties of both the fractured matrix and the karst conduits [e.g., *Dershovitz et al.*, 1991]. The second approach consists in using double-continuum models to simulate flow exchanged between the systems based on differences in hydraulic head via linear exchange terms [*Barenblatt et al.*, 1960; *Teutsch*, 1988, 1989; *Sauter*, 1992]. A third approach couples discrete flow path networks to a continuum in order to model dualistic flows in MFKS (''hybrid models'') [*Kiraly*, 1984; *MacQuarrie and Sudicky*, 1996; *Arfib and de Marsily*, 2004]. *Liedl et al.* [2003] used such an approach by coupling a pipe network with a fractured system via linear exchange terms, with simulations of Darcian flow in the matrix done using a finite difference scheme. The first and third approaches require a good knowledge of either the fracture systems or the location of the karst conduits, hydrodynamic properties and geometry. In most cases, this information is not available and only the second approach can actually be used.

[24] In the double-continuum modeling methodology described here, the karst system has therefore been conceptualized by two interacting free-surface water reservoirs (Figure 8): reservoir 1 corresponds to the conduit network and reservoir 2 to the matrix.

3.2. Reservoir 1: The Conduit Network

[25] The conduit system (reservoir 1) is characterized by relatively high flow velocities but low storage capacity at the basin scale. Depending on the magnitude of the flow velocity, either laminar or turbulent flow may occur in individual conduits. In the present approach, the conduit network is assumed to be very transmissive compared to the matrix. The hydraulic gradient is, therefore, assumed to be negligible in the conduits and consequently hydraulic head is assumed to be the same throughout the entire conduit network both under natural flow conditions and during the pumping test. Reservoir 1 is assumed to be a free-surface reservoir as water levels can fluctuate in vertical shafts and variably saturated solution conduits, as illustrated in Figure 7.

[26] Reservoir 1 (Figure 8) is recharged by inflow from Buèges river losses (L), from the Hérault river (Q_R) when the hydraulic head in the conduit is lower than the water level in the river, while the pumping flow rate (P) is abstracted from this reservoir. Exchanges with reservoir 2 (β) depend on the respective hydraulic heads in the two reservoirs. The hydraulic head in reservoir 1 (h_c) is assumed to be the same throughout the entire conduit network and limited by a threshold value (Th_c) that corresponds to the elevation of the spring, above which the reservoir overflows, inducing a discharge at the spring (Q_S). In reservoir 1, under given initial conditions and specified boundary conditions, the model computes the hydraulic head in the conduits h_c and the discharge rate at the spring Q_S, integrating equation (3) and using physical data and parameters (Table 2).

[27] Assuming a porosity $\phi_c = 1$ in the conduit network, the equation of volume conservation in this reservoir is:

$$\frac{dh_c}{dt} = \frac{\beta + Q_R + L - Q_S - P}{S_c} \tag{3}$$

where S_c is the free-surface area of dewatering conduit network (vertical shafts and variably saturated conduits).

3.3. Reservoir 2: The Matrix

[28] Reservoir 2 corresponds to the matrix drained by the conduit network (reservoir 1). It is supplied by recharge (R) from epikarst after rainy events and/or by infiltration through fractures or fissures within the karst massif. The diffuse flow (β) exchanged between reservoirs 1 and 2 is

Table 2. Parameters of Reservoir 1

Data	Parameter/Data and Unit	Description	Fixed/Fitted
Parameters	S_c (m^2)	Free-surface area of dewatering conduit network	Fitted during calibration
	Th_c (m)	Threshold hydraulic head in the conduit beyond which the spring overflows	Fixed (measured)
Initial condition	h_{c0} (m)	Initial hydraulic head in the conduit	Fixed (measured)
Boundary conditions	L (t) (m^3/s)	Discharge flow of losses	Fixed (monitored)
	Q_R (t) (m^3/s)	Discharge flow from river	Fixed (monitored)
	P (t) (m^3/s)	Pumping flow rate	Fixed (monitored)
	β (t) (m^3/s)	Exchange flow rate	Fixed (calculated by reservoir 2)
Results	h_c (t) (m)	Hydraulic head in the conduit	Calculated by reservoir 1
	Q_S (t) (m^3/s)	Spring flow rate	Calculated by reservoir 1

computed assuming Darcian flow in the matrix considered as an equivalent porous media and is a function of the difference in hydraulic head between the two reservoirs (see the following paragraph). As a first approximation, the hydraulic head in the free-surface reservoir 2 (h_m) is assumed to be the same throughout the entire karst basin.

[29] Equation of volume conservation in this reservoir is:

$$\frac{dh_m}{dt} = \frac{R - \beta}{\phi_m A} \tag{4}$$

where A is the surface area of the karst basin (excluding the watershed supplying the Buèges River losses) and ϕ_m is the specific yield (drainage porosity) of the free-surface matrix.

3.4. Exchange Flow

[30] Under natural conditions, the exchanged flow $\beta(t)$ between the matrix and the conduit network results from the natural hydraulic heads difference between the two reservoirs. During low flow conditions, this flow corresponds to the recession flow measured at the spring minus the Buèges river losses. During the pumping test, the hydraulic head decreases in the conduits and the difference in hydraulic head increases. Assuming that during the test the drawdown in the matrix is negligible compared to the drawdown in the conduits, according to the principle of superposition [*de Marsily*, 1986], the total flow exchanged between the matrix and the conduits is equal to the sum of the natural flow Q_α that is due to the natural difference in hydraulic head between the matrix and the conduits and the flow Q_{IND} that is due to the additional drawdown induced by the pumping:

$$\beta(t) = Q_\alpha(t) + Q_{IND}(t) = Q_0 e^{-\alpha t} + Q_{IND}(t) \tag{5}$$

where Q_α (t) = Q_0 $e^{-\alpha t}$ is natural diffuse flow from the matrix to the conduit network, corresponding to the base flow of the spring according to the *Maillet* [1905] formula minus Buèges River losses ($Q_\alpha(t) = Q_S(t) - Q_L(t)$, Figure 3). According to equation (5), this flow can be estimated knowing the recession coefficient α and an initial discharge Q_0 at the spring.

[31] The induced flow exchange is usually computed from differences in hydraulic head using linear exchange terms [*Barenblatt et al.*, 1960]. In the present approach, the matrix is assumed to behave as an equivalent porous medium. Because the measured drawdowns are low (<25%) compared to the total thickness (several hundred of meters) of the saturated matrix aquifer, the application of analytical solutions for confined aquifer is possible without introducing any inaccuracy. An analytical solution of prescribed hydraulic

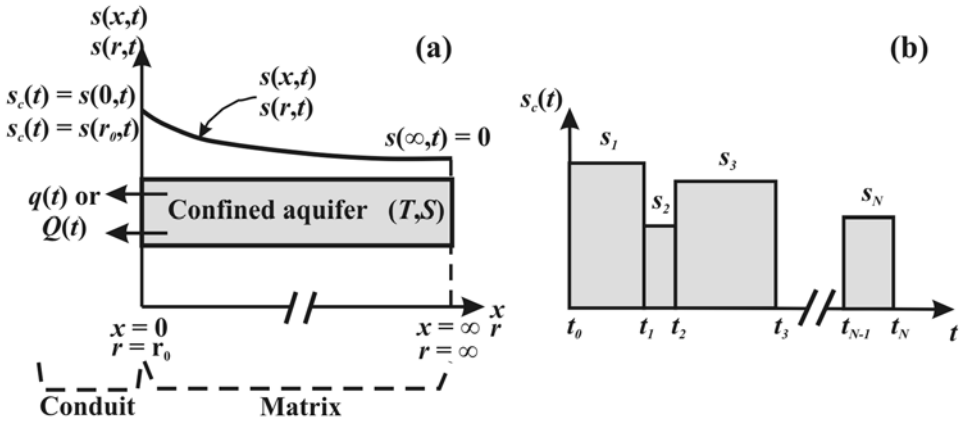

Figure 9. (a) Sketch of 1D-linear (coordinate x) or 2D-radial (coordinate r) flow toward a trench or a well; (b) varying drawdown imposed on the conduits network.

Table 3. 1-D and 2-D Analytical Solutions of Transient Flow Under Constant and Varying Drawdown

	One-Dimensional Flow	Radial Flow
Constant drawdown	$Q(t) = \frac{l}{\sqrt{\pi}}\sqrt{\frac{TS}{t}}\, s_c$ (7)	$Q(t) = 2\pi T s_c G(a)$, $a = \frac{Tt}{Sr_o^2}$ (8)
Varying drawdown	$Q_{IND}(t) = 2l\sqrt{\frac{ST}{\pi}}\left\{\sum_{i=1}^{N+1}\frac{(s_i - s_{i-1})}{\sqrt{t-t_{i-1}}}H(t-t_{i-1})\right\}$ with $s_0 = 0$ and $s_{N+1} = 0$ (9)	$Q_{IND}(t) = 2\pi\, T\left\{\sum_{i=1}^{N+1}(s_I - s_{I-1})G(a_{I-1})H(tt_{I-1})\right\}$ with $s_0 = 0$ and $s_{N+1} = 0$ $G(a_j) = \frac{4a_j}{\pi}\int_0^\infty ue^{-\alpha j\ u2}\left\{\frac{\pi}{2} + arctan\left[\frac{Y_o(u)}{J_o(u)}\right]\right\} du$ where $a_j = \frac{T(t-t_j)}{Sr_0^2}$ for j = to N (10)
Parameters	l length of the trench (karst conduit network)	r_0 radius of the well (karst conduits); $G(a)$ well production function; a dimensionless time; J_0 and Y_0 first- and second-kind, zero-order Bessel functions respectively, and u dummy variable
	T transmissivity of the aquifer (matrix); S storage coefficient of the aquifer (matrix); s_c constant drawdown at the trench or well (conduits);	

head boundary condition type can be used depending on the assumed geometry of diffuse flow: 1D-flow (solution toward a trench, [*Jenkins and Prentice*, 1982]) or 2D-radial flow (solution toward a well, [*Jacob and Lohman*, 1952]).

[32] The evolution of flow with time t, in a trench or in a well draining a confined aquifer (Figure 9a), where a sudden drawdown s_c is assigned at time $t = 0$, is given by analytical solutions (7) and (8) in Table 3. Given that drawdown in the conduit is not constant but varies with time, this relationship was implemented using the principle of superposition. The varying drawdown $s_c(t)$ at the conduit can be discretized in the time domain as a series of discrete drawdowns s_1, s_2, $s_3 \ldots s_N$ (Figure 9b).

[33] The following boundary condition in the conduit is assumed:

$$s_c(t) = \sum_{i=1}^{N} s_i(H(t-t_{i-1}) - H(t-t_i)), H(t-t_0) = 1 \text{ with } t_0 = 0 \tag{6}$$

where $H(u)$ is the Heaviside step function ($H(u) = 0$ if $u < 0$, $H(u) = 1$ if $u \geq 0$).

[34] Applying the principle of superposition (Appendix A), the induced diffuse flow under varying drawdown in the conduit is given by equations (9) for 1-D flow and (10) for 2-D radial flow in Table 3. The data and parameters used in reservoir 2 are summarized in Table 4.

[35] The various flow components are computed at each time step in both reservoirs while the volume conservation differential equations are integrated on time.

4. Modeling Results

4.1. Model Calibration

[36] Due to the fact that the s_m/s_c ratio is lower than 0.10 during the entire long-duration pumping test, drawdown in the matrix is assumed to be negligible compared to drawdown in the conduits. Therefore equations (9) of one-dimensional flow toward a trench and (10) of radial flow toward a well as described above have been used to calculate flow exchange. Given that quadratic head losses in the conduit cannot be precisely located and are negligible compared to the total drawdown in the well, they are not explicitly considered in the model. Equations (3) and (4) of volume conservation in reservoirs 1 and 2 and the calcula-

Table 4. Parameters of Reservoir 2

Data	Parameter and Unit	Description	Fixed/Fitted
Parameters	A (m^2)	Surface area of the karst basin (excluding the watershed of the losses)	Fixed (measured)
	Q_0 (m^3/s)	Initial base flow rate at time t = 0	Fixed (measured)
	α (1/d)	Recession coefficient	Fixed (measured)
	$S_m = \phi_m$ (−)	Storage coefficient of matrix (=drainage porosity)	Fitted during calibration
	T_m (m^2/s)	Transmissivity of matrix	Fitted during calibration
	l (m) or r_0 (m)	Length (1D) or radius (2D) of the conduit network according to flow dimension	Fitted during calibration
Initial condition	h_{m0} (m)	Initial hydraulic head in the matrix	Fixed (measured)
Boundary condition	$R(t)$ (m^3/s)	Recharge rate	Fixed (monitored) – $R = 0$ during recession season
Results	$\beta(t)$ (m^3/s)	Exchange flow rate	Calculated by reservoir 2
	$h_m(t)$ (m)	Hydraulic head in the matrix	Calculated by reservoir 2

Table 5. Parameters, Initial and Boundary Conditions of the Calibrated Model Giving the Best Matching of Measured Drawdown in the Conduit

Data	Reservoir 1 (Conduits)	Reservoir 2 (Matrix)
Parameters	S_c = 1900 m^2, calibrated Th_c = 76.9 m, measured	A = 30 km^2, measured [*Aquilina et al.*, 2005] $S_m = \phi_m$ = 0.007, calibrated T_m = 1.6 × 10^{-5} m^2/s, calibrated l = 5000 m, calibrated Q_0 = 0.240 m^3/s measured at the spring α = 0.0021 d^{-1} estimated from discharge measurements time series at the spring before the test
Initial conditions	h_{c0} = 76.9 m, measured at the well	h_{m0} (m) = 110 m, measured at well P6
Boundary conditions	L = 0.015 m^3/s, measured by differential gauging Q_R = 0.030 m^3/s if h_C < 75 m, estimated using chemical mixing theory applied to the pumped water P (m^3/s) = Series measured during the test	R = 0 m^3/s estimated during low flow conditions

tion of Q_{IND} are solved using the MATLAB/SIMULINK code starting at time t = 0 on 27 July 2005 at 6 AM with a time step of one hour.

[37] The model was calibrated by adjusting four parameters (Table 5) to modify model output so that model results match field observations within an acceptable level of accuracy. The parameters adjusted during the calibration process are the hydraulic transmissivity and storage coefficient of the matrix, the total length of the karst conduit network and the free-surface area of dewatered karst conduits. After each change in one of these parameters, the model was run, and simulated water levels in reservoir 1 were compared to measured water levels in pumping well F3. For each run, the model accuracy was calculated using the relative root mean square (rRMS) error between measured drawdown and simulated drawdown. Model accuracy is increased by minimizing the rRMS error. As previously explained at section 2.3, the approach is focused on the response in the karst conduit. Nevertheless, during the entire calibration process, the measured drawdown in the matrix (at P5, P6 and P7) was compared to simulated drawdown in reservoir 2 in order to check that the calibration process focused on the pumping well in the karst conduit does not lead to abnormal simulated drawdown in the matrix. This part of the calibration enables to estimate the storage coefficient (S_m) in the matrix, the calibration of drawdown in the karst conduits leading only to the product $\sqrt{T_m S_m}$ according to equation (9).

[38] The calibrated model results are shown in Figure 10. In reservoir 1, the fit of the model to measured data is very good during the whole test (rRMS = 2.3 % at well F3) and especially remarkable during the recovery observed after the

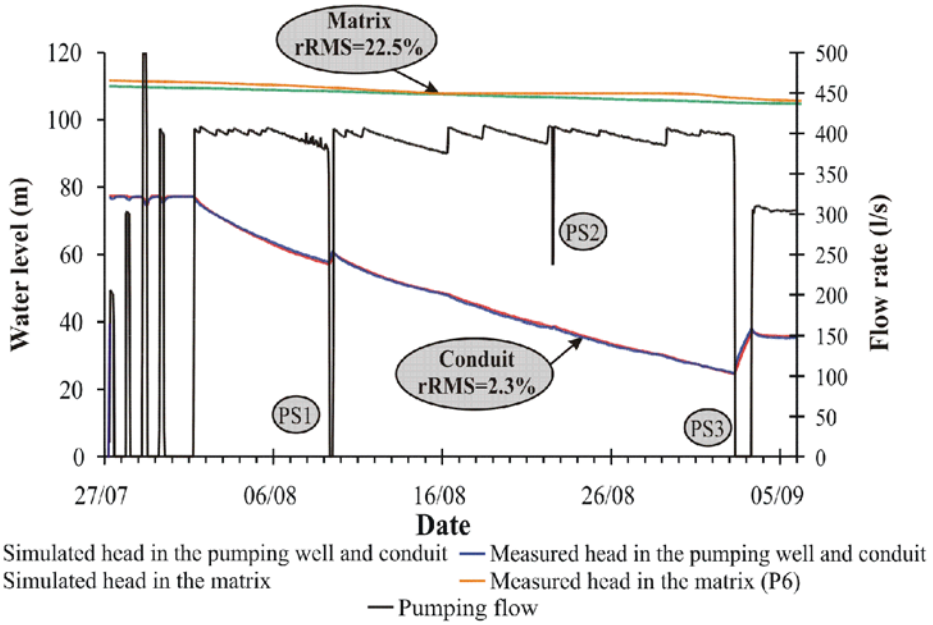

Figure 10. Temporal evolution of simulated and measured drawdown in the conduit and in the matrix using the solution of one-dimensional flow toward a trench for exchange flow rate (rRMS is computed on drawdown referred to initial water level; PS: pump stop).

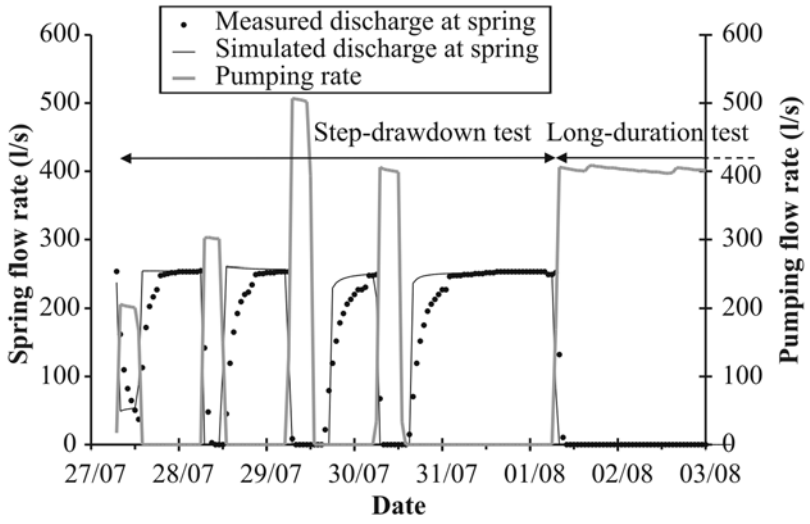

Figure 11. Measured and simulated discharge flow rate at the spring.

pumping stop at the beginning of September 2005 (pump stop PS 3 in Figure 10) and during the following step at 0.3 m^3/s. This last part of the test was the most difficult to simulate using other analytical solutions for flow exchange calculation. Simulations using equation (10) for radial flow in the matrix or the classical linear exchange of flow between matrix and conduits [*Barenblatt et al.*, 1960] did not allow to match the measured drawdown. This and the good calibration obtained with equation (9) suggest the existence of one-dimensional flow conditions into the matrix. The conduit network acts as a trench network draining the matrix with Darcian parallel flows. The calibrated parameters obtained and initial and boundary conditions of the calibrated model are summarized in Table 5. In reservoir 2, the simulated drawdown roughly follows the measured drawdown at observation wells P5, P6 (Figure 10), and P7 in the matrix with an average of the three rRMS equal to 22.5%. This match is less satisfactory than in reservoir 1 due to the assumption of an equal hydraulic head in reservoir 2 while drawdown spatially fluctuates due to local heterogeneities in the matrix and real distance between the piezometers and the conduit network.

[39] The discharge at the spring varies much (Figure 11) during the pumping tests, with alternating periods of flow and periods of drying-up. The model simulates quite well the fluctuations in the spring discharge rate. The model reacts (and recovers) a bit too strongly to pumping stops as a consequence of the assumption that at each time step the total amount of water surplus above the spring threshold (Th_c) is allocated to simulated spring discharge. In fact, the flow rate at the spring is limited by karst conduit constriction. Measured flow at the spring is, therefore, systematically lower than the flow simulated during recovery periods. This output of the model can be improved while calculating the spring flow with the existing measured rate curve between hydraulic head in the conduit and discharge rate at the spring.

4.2. Sensitivity Analysis

[40] The free-surface area of the karst conduits S_c can be accurately calibrated during periods when the pumping rate changes (pump stops PS1 to PS3 in Figure 10) and/or recovery periods, which were designed partly for this purpose. The value obtained (1900 m^2) allows a very good fitting of the recovery after the pumping stop (PS3) on 9 August 2005 and of the effects of other stops or pumping rate changes (PS1 and PS2). It is not necessary to introduce a variation of this parameter with the hydraulic head in the conduits. This suggests the absence of any major change in porosity (and therefore geometry) of vertical shafts and variably saturated conduits with depth at the scale of the karst basin, at least within the range of hydraulic heads investigated during the pumping test. The sensitivity analysis

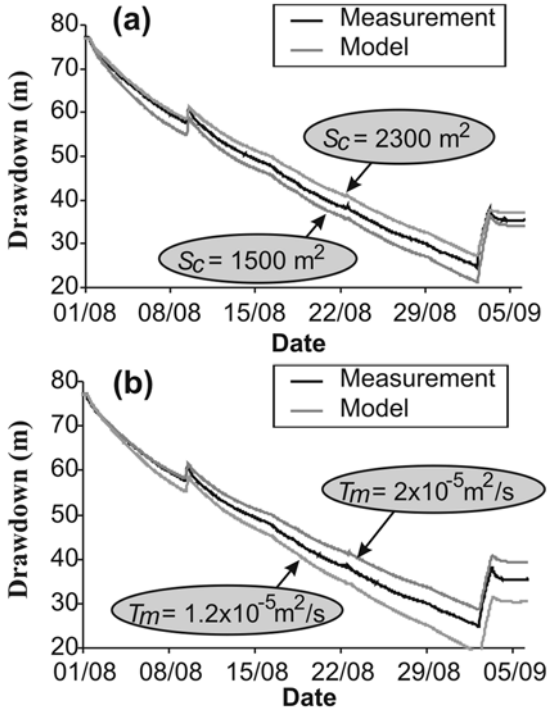

Figure 12. Sensitivity analysis on (a) free surface area of dewatering conduit network and (b) transmissivity of matrix.

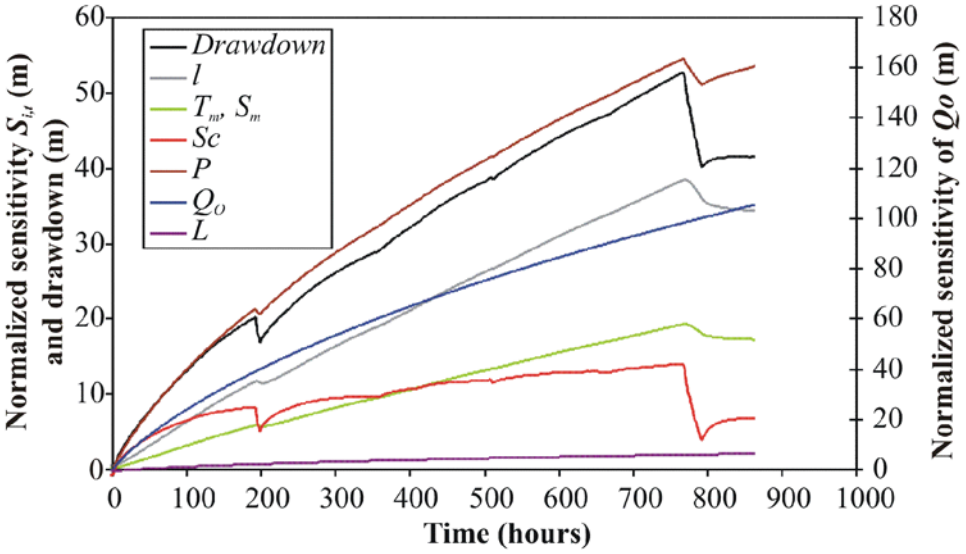

Figure 13. Systematic sensitivity analysis of model parameters and flow rates.

of this parameter shows that it is well constrained: 1900 ± 100 m^2 (a variation of ±400 m^2 is shown in Figure 12a for clarity).

[41] The length of the conduit network is an unknown parameter of the karst system. It is assumed to be at least about 5-km long on the basis of the shape of the karst system and the distance between the spring and the Buèges River losses. The transmissivity obtained (T_m = 1.6 ± 0.1 E-05 m^2/s, a variation of ±0.4 E-05 m^2/s is illustrated in Figure 12b for clarity) for the matrix is quite low and is responsible for the large drawdown measured during the pumping test. This also means that the connection between the matrix and the conduit network is not very efficient. This value is determined at the scale of the karst basin for a matrix intersecting a 5-km long conduit network.

[42] A systematic sensitivity analysis was done to determine the effect of parameters and flow rates uncertainty on the hydrodynamics of the system during the test. Sensitivity is defined as the rate of change in one factor with respect to a change in another factor. The normalized sensitivity is used to compare parameters and is defined as [*Kabala*, 2001]

$$S_{i,t} = \frac{\partial O}{\partial P_i / P_i} = P_i \frac{\partial O}{\partial P_i} \tag{11}$$

where $S_{i,t}$ is the normalized sensitivity of i^{th} input parameter at time t, O is the output function of the system (i.e., the karst conduit drawdown at F3 in this case) and P_i is the ith input parameter of the system (in our case: S_c, T_m, S_m, l, L, Q_0). The partial derivative of this equation can be approximated by a forward differencing formula as [*Huang and Yeh*, 2007]

$$\frac{\partial O}{\partial P_i} = \frac{O(P_i + \Delta P_i) - O(P_i)}{\Delta P_i} \tag{12}$$

[43] The increment in the denominator was approximated by multiplying the parameter value by a factor of 10^{-2}, i.e., $\Delta P_i = 10^{-2} P_i$. Equation (12) measures the influence that the fractional change in a parameter, or its relative error, exerts on the output [*Huang and Yeh*, 2007].

[44] The normalized sensitivity of all the parameters starts at the beginning of the pumping (Figure 13), which shows that all the parameters contribute to the drawdown. The drawdown is very sensitive to the natural contribution of the matrix (Q_0), its relative sensitivity Q_0 being the highest of all from 60 h to the end of the test. The normalized sensitivity of the pumping rate (P) is also high, which means that interpreting such a pumping test requires a very accurate knowledge of the flow components soliciting the karst conduits (especially pumping rate and natural contribution of the matrix). Logically, drawdown is particularly sensitive to T_m and S_m, except at the beginning of pumping. The normalized sensitivity of these parameters increases continuously until the end of pumping. At the beginning of pumping, drawdown is more sensitive to the storage in the conduits (S_c) than to T_m and S_m. After a very rapid increase, the sensitivity of S_c stabilizes after about 150 h. Such a phenomenon is consistent with the physical behavior of the system characterized by a capacity effect due to the karst conduits. After about 100 h, the sensitivity of the length (l) of the conduit network (although it remains low in absolute value) becomes higher than the sensitivity of storage in the conduits (S_c). This is due to the linear dependence on the parameter l of the total discharge of exchange flow between the matrix and the conduits. The evolution with time of sensitivities outlines the progressive increase of the influence of exchange flow from the matrix on the drawdown into the conduits.

5. Discussion

5.1. Comparison With Vertical Fracture Solution

[45] Geometrical similarities suggest that the analytical solution for a well intersecting a vertical fracture of infinite conductivity with a storage effect [*Gringarten et al.*, 1974; *Ramey and Gringarten*, 1976] could be applied to the present case of pumping in a karst conduit. The log-log diagnostic plot (Figure 6) also suggests that kind of hydraulic behavior [*Renard*, 2005]. This solution was developed by petroleum engineers for its application to artificially

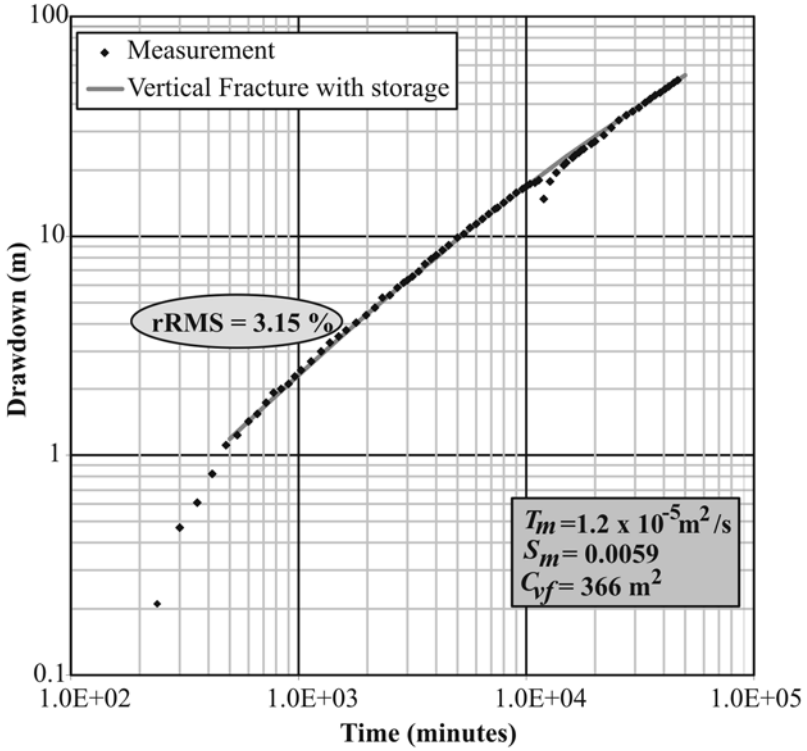

Figure 14. Temporal evolution of measured drawdown and fitting with the single vertical fracture method of *Ramey and Gringarten* [1976].

fractured wells [*Kruseman and de Ridder*, 1991]. The analytical solution deals with a fully penetrating, vertically fractured well pumped at a constant rate, in an ideal, homogeneous, and horizontal formation (corresponding to the matrix in the karst system) of constant thickness, porosity (S_m) and permeability (T_m). The fracture is idealized as a planar surface of zero thickness and infinite hydraulic conductivity such that there is no hydraulic head drop as water flows internally through the fracture to the well. In addition, it is assumed that the well is large enough to induce a significant well storage effect. This storage volume involves all the high-hydraulic conductivity volumes which communicate with the well [*Ramey and Gringarten*, 1976]. It is represented by C_{vf} defined as the ratio between the change in volume of water in the well plus vertical fracture, and the corresponding drawdown (to be compared to S_c in the numerical model). Although it is cited in hydrogeology literature, field examples of this analytical solution are rare [*Kruseman and de Ridder*, 1991].

[46] The matching of measurements with this analytical solution is satisfactory (Figure 14) with rRMS = 3.15 %. The hydrodynamic parameters obtained with the same length characteristic (5000 m for the fracture) are for the most part similar to those obtained using the numerical model (Tables 1 and 5). The main difference concerns the storage parameter in the karst conduits (C_{vf} = 366 m^2 whereas S_c = 1900 m^2), which seems to be underestimated with the analytical solution. This is probably due to small geometrical discrepancies: assumption of pseudo-radial flow to the fracture in the analytical solution and one-dimensional flow in the numerical model. The slope (0.70) of the straight line on the log-log diagnostic plot (Figure 6) at late times suggests that the flow in the matrix tends to be one-dimensional and not pseudo-radial as already suggested by the numerical model. Since the storage in the karst conduits is very sensitive to changes in the pumping rate, the numerical model developed for varying pumping rates is more sensitive to this parameter than the analytical solution. The value obtained with the numerical model is, therefore, definitely more reliable. Nevertheless, the vertical fracture model leads to the only simple analytical solution which is physically based and provides satisfactory results as a preliminary approach for the interpretation of such a type of pumping test.

5.2. Flow Components

[47] The numerical model enables to determine the temporal evolution of the various contributing flows during the pumping test (Figure 15): the sum of the pumping rate and the spring discharge results from the natural contribution of the matrix, the additional flow from the matrix due to the pumping, the Hérault river contribution, the Buèges river losses contribution and the dewatering of the karst conduit network.

[48] According to the recession function incorporated in the model, the natural flow from the matrix decreases exponentially from Q_0 = 0.240 m^3/s at the beginning of the pumping down to about 0.219 m^3/s at the end of the test.

[49] The additional flow from the matrix induced by pumping increases with time along with the drawdown from Q_{IND} = 0 m^3/s at the beginning of pumping (no induced flow) and up to 0.105 m^3/s (maximum induced flow) at the end of the 0.4 m^3/s pumping step. This evolution is confirmed by the hydrochemical monitoring of the pumped water, the relationship between $^{87}Sr/^{86}Sr$ and

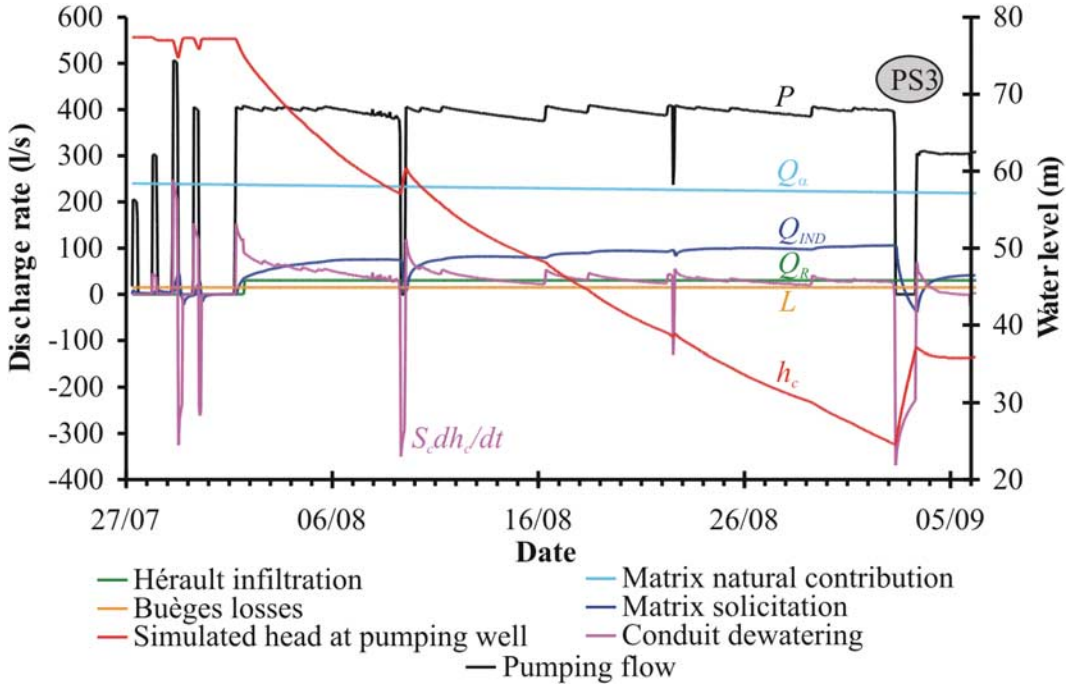

Figure 15. Temporal evolution of the flow contributions simulated by the model during the pumping test (discharge flow Q_S at the spring is not presented for clarity).

the Cl/Sr ratios enabling to distinguish the different end-members: Hérault River water, Buèges River losses and groundwater from the dolomite matrix. During the pumping test, the signature of the pumped water tends toward the signature of the dolomite end-member, which suggests a larger contribution of water from the matrix [*Ladouche et al.*, 2005]. The diffuse flow decreases rather quickly after each pumping stop due to recovery in the conduits, and becomes negative during pump stop PS3 when the hydraulic head in the conduit rapidly increases and inverts the hydraulic gradient between matrix and conduits. In that case, the karst conduits recharge the matrix ($Q_{IND} < 0$), similar to what happens during recharge of the aquifer during high-flow periods.

[50] The dewatering of the conduit network is the lowest flow component (Figure 15). It decreases with time, proportionally to the decreasing rate of depletion in the conduits. Obviously, the dewatering volume is proportional to the drawdown in the conduit network, whatever the value of drawdown. The dewatering fluctuates between 0.150 m^3/s at the beginning of the test and about 0.020 m^3/s at the end of the pumping test at 0.400 m^3/s. It suddenly increases after each increase in the pumping rate due to the associated increase in the drawdown rate. It becomes negative during pumping stops PS1 to PS3, when the hydraulic head in the conduit increases and water from the matrix (and other contributions) is stored in the conduit network (dewatering flow is negative).

[51] The integration of the various flows calculated by the model during the long-duration pumping test (1 August to 6 September 2005) enables to quantify the different volumes mobilized during the test (Table 6). In order to determine the efficiency of the pumping, the ratio E between the total pumped volume and what would have been the natural flow in the karst system (Buèges River losses + natural matrix contribution) during the same period, we defined:

$$E = \frac{\int_0^\tau P(t)dt}{\int_0^\tau L(t)dt + \int_0^\tau Q_\alpha(t)dt} \tag{13}$$

where τ is the duration of the pumping test.

[52] The ratio E represents the increase in available water due to pumping. For the August 2005 pumping test, this ratio is 1.54, which corresponds to a 54 % increase in the

Table 6. Origin of Total Pumped Volumes During the Long-Duration Pumping Test (1 August–6 September 2005)

Type	Flow Component	Volume, m^3	Contribution to Total, %	Contribution to Total, %
Natural	Matrix natural contribution	710,165	60.8	64.8
	Buèges losses	46,710	4.0	
Induced by pumping	Matrix induced flow	239,864	20.5	35.2
	Hérault infiltration	92,124	7.9	
	conduits dewatering	78,525	6.7	
	Total	1,167,387	100	100

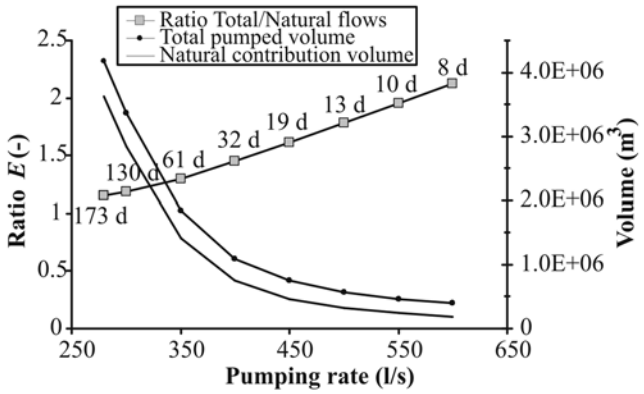

Figure 16. Exploitation volumes simulations at different pumping rates before dewatering of the pump at a depth of 54 m (pumping duration is given in days).

water flowing from the aquifer due to pumping. If we consider that infiltration from the Hérault River does not participate in the yield of the karst aquifer, the ratio E is 1.46.

[53] Table 6 suggests that the flow exchange between matrix and conduits (sum of natural and induced matrix flow) represents more than 80 % of the flow pumped at the well. In addition to its role in karst genesis [*Bauer et al.*, 2003], flow exchange constitutes the main source of water during MFKS exploitation.

5.3. Simulations

[54] Another advantage of the modeling tool described here is that it can simulate various pumping scenarios in order to assess the potential exploitation of the karst system through pumping in the well tapping the conduit. Simulations of pumping at constant discharge rates have been done using the calibrated model for several discharge values (0.280, 0.3, 0.35, 0.4, 0.45, 0.5, 0.55, and 0.6 m^3/s). The maximum pumping duration (before reaching the maximum drawdown of 54 m imposed by the pump depth) was calculated along with the pumped volumes (Figure 16) and the efficiency ratio E. Other simulations were performed, including one for a deeper well according to the geometry of the conduit network.

[55] The maximum pumping duration increases as the pumping rate decreases. The absolute pumped volume is the greatest when the pumping rate is low, because this pumping context involves a longer solicitation of the matrix and generates drawdowns in the matrix that propagate farther from the conduit network. However, the pumping efficiency is greater with higher pumping rates because during short duration pumping, the relative natural contribution from the karst is lower, i.e., $E = 2.12$ for an 8 day pumping test at 0.6 m^3/s, but in this case the pumped volume before dewatering of the pump is quite low.

[56] At the end of the August 2005 pumping test, the discharge rate has been reduced from 0.4 to 0.3 m^3/s during four days. During this period, the hydraulic head in the conduit seemed to stabilize at an elevation of 36 m for several days (Figure 10). Thereafter, very heavy rainfall occurred, perturbing the test and the recovery. The model was used to simulate what would have happened if pumping had continued at 0.3 m^3/s without any rainfall. This simulation (Figure 17) shows that after an apparent stabilization period lasting a few weeks, the drawdown would have again increased in the conduit. The "pseudo stabilization" observed during the 0.3 m^3/s step is temporary and results from the superposition of the effects of the "recovery" due to the 0.4 m^3/s pumping stop with the drawdown due to the next 0.3 m^3/s pumping step.

[57] This absence of long-term stabilization is related to the fact that the analytical solution used does not take into consideration any fixed head or recharge boundary, which is in agreement with observations during the pumping test (absence of drawdown stabilization and hydrogeological knowledge of the karst system), but does not foresee the true behavior of the system over the longer term. Actually, for very long term use, the model is therefore somewhat pessimistic because during a hydrological cycle the system would be recharged by rainfall. An improved version of the model is therefore being developed in which the natural

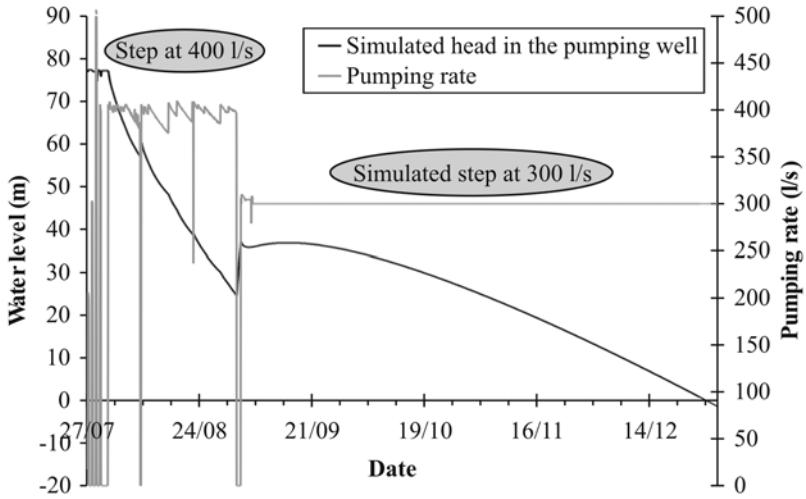

Figure 17. Hydraulic head simulated at the pumping well with a longer step at 300 l/s without any recharge (until 31 December 2005).

contribution of the karst system during recharge periods is taken into account.

6. Conclusion

[58] The hydrodynamics of a mixed flow karst system (MFKS) in which a long-duration pumping test has been done on the main karst conduit was analyzed and modeled. These results show that both the matrix (several kilometers away from the pumping well) and the conduit network are affected by the test. Nevertheless, the conduits are much more affected by pumping than the matrix (drawdown in the conduits ten times higher than drawdown in the matrix) due to their better connection to the pumping well and their low storage capacity at the basin scale.

[59] The double continuum model composed of two reservoirs (conduit network and matrix) well reproduces the transient response in the pumping well. The sensitivity analysis shows that it is the low-permeability matrix that dictates the pumping test response. The conduits induce a moderate capacitive effect (dewatering of vertical shafts and variably saturated conduits).

[60] The developed methodology also constitutes a useful tool for improving the knowledge of the karst system and identifying the various flow components reaching the pumping well. This approach can also be implemented with various flow types in the matrix considered as an equivalent porous media. Free of deterministic finite difference/elements modeling, it is simpler than hybrid models and constitutes an advance in double continuum modeling of karst systems notably by an improvement in the calculation of the flow exchange rate between matrix and conduits. It can also be used to prepare a pumping test. It shows, among others, the necessity of programming some recovery phases and significant pumping discharge changes during the pumping test.

[61] Such a model offers a wide possibility of practical applications as most karst water resources in the world are of the MFKS-type and are easily attainable only by pumping in the conduit located directly above the main outlet of the aquifer.

Appendix A

A1. 1D-Solution

[62] Consider the problem of 1D-flow toward a trench under varying drawdown. The 1D form of the diffusion equation is

$$S\frac{\partial s}{\partial t} = T\frac{\partial^2 s}{\partial x^2} \tag{A1}$$

with the initial and boundary conditions

$$s(x,0) = 0,\ s_c(t) = s(0,t),\ \frac{\partial s}{\partial x}(\infty,t) = 0 \tag{A2}$$

where the symbols stand for aquifer transmissivity (T), storage coefficient (S), time (t), drawdown (s), axial coordinate (x) and drawdown at the trench (s_c).

[63] The boundary condition at the trench are given by equation (4).

[64] After computation of the pulse response $s^*(x, t)$ and convolution with $s_c(t)$ by Laplace transformation, then inverse transform, we find the drawdown function $s(x, t)$.

[65] The discharge rate per unit of trench length is then obtained by

$$q(t) = \lim_{x\to 0} T\frac{\partial s(x,t)}{\partial x} \tag{A3}$$

[66] Hence:

$$q(t) = \sqrt{\frac{ST}{\pi}}\left\{\frac{s_1}{\sqrt{t}} + \frac{(s_2 - s_1)}{\sqrt{t - t_1}}H(t - t_1) + \frac{(s_3 - s_2)}{\sqrt{t - t_2}}H(t - t_2) + \frac{(s_4 - s_3)}{\sqrt{t - t_3}}H(t - t_3) + \ldots\right\} \tag{A4}$$

or

$$q(t) = \sqrt{\frac{ST}{\pi}}\left\{\sum_{i=1}^{N+1}\frac{(s_i - s_{i-1})}{\sqrt{t - t_{i-1}}}H(t - t_{i-1})\right\} \quad \text{with } s_0 = 0,\ s_{N+1} = 0 \text{ and } t_0 = 0 \tag{A5}$$

[67] If $t_1 = \infty$, we find the transient solution under a constant drawdown [*Ferris et al.*, 1962; *Jenkins and Prentice*, 1982]:

$$q(t) = \sqrt{\frac{ST}{\pi t}}s \tag{A6}$$

[68] The above solution, equivalent to equation (7) from Table 3, is the formula used to estimate the transient discharge rates at a trench under constant drawdown.

A2. Radial Solution

[69] Confined horizontal flow toward a fully penetrating well is classically described by the radial form of the diffusion equation

$$S\frac{\partial s}{\partial t} = \frac{1}{r}\frac{\partial}{\partial r}\left(rT\frac{\partial s}{\partial r}\right) \tag{A7}$$

with the initial and boundary conditions

$$s(r,0) = 0,\ s_c(t) = s(r_0,t),\ \frac{\partial s}{\partial x}(\infty,t) = 0 \tag{A8}$$

where r is the radial coordinate and r_0 the well radius.

[70] The same approach as above leads to the following solution

$$Q(t) = 2\pi T\{s_1 G(\alpha_0)H(t - t_0) + (s_2 - s_1)G(\alpha_1)H(t - t_1) + (s_3 - s_2)G(\alpha_2)H(t - t_2) + \ldots - s_N G(\alpha_N)H(t - t_N)\} \tag{A9}$$

or

$$Q(t) = 2\pi T\left\{\sum_{i=1}^{N+1}(s_i - s_{i-1})G(\alpha_{i-1})H(t - t_{i-1})\right\} \text{with } s_0 = 0 \text{ and } s_{N+1} = 0 \tag{A10}$$

$$\text{with } G(\alpha_j) = \frac{4\alpha_j}{\pi}\int_0^\infty u e^{-\alpha_j u^2}\left\{\frac{\pi}{2} + \arctan\left[\frac{Y_o(u)}{J_o(u)}\right]\right\}du, \quad \text{(A11)}$$

where $\alpha_j = \frac{T(t-t_j)}{Sr_0^2}$ for $j = 0$ to N, $\alpha_0 = \frac{Tt}{Sr_0^2}$ if $t_0 = 0$ with J_0 et Y_0 are first- and second-kind, zero-order Bessel functions respectively, and u is a dummy variable.

[71] If $N = 1$, then the drawdown at the well is $s = s_1$ during t_1, and afterward $s = 0$, we find:

$$Q(t) = 2\pi T s_1\{G(\alpha_0) - G(\alpha_1)H(t - t_1)\} \quad \text{(A12)}$$

which is the solution of a cycle composed of a solicitation phase followed by recovery.

[72] If $t_1 = \infty$, we find the classical transient solution under a constant drawdown:

$$Q(t) = 2\pi T s_1 G(\alpha) \quad \text{(A13)}$$

[73] The above solution, which is the reference formula used to evaluate the transient discharge rates at a well, or a tunnel, under a constant drawdown [*Jacob and Lohman*, 1952], is equivalent to equation (8) from Table 3.

[74] **Acknowledgments.** This research project was funded by BRGM within the framework of the EAUR15 COMPLEX'AQUI project and the Conseil Général de l'Hérault, France. The authors thank Sandra Lanini and Pierre Perrochet for their contribution to the implementation of the superposition principle in the numerical model. The comments of two anonymous reviewers were greatly appreciated.

References

Aquilina, L., B. Ladouche, M. Bakalowicz, R. Schoen, and E. Pételet (1999), Caractérisation du fonctionnement des systèmes karstiques nord-montpelliérains - Volume de synthèse générale, *Report R40746*, 50 pp., BRGM, Montpellier, France.

Aquilina, L., B. Ladouche, and N. Dörfliger (2005), Recharge processes in karstic systems investigated through the correlation of chemical and isotopic composition of rain and spring-waters, *Appl. Geochem.*, *20*, 2189–2206.

Aquilina, L., B. Ladouche, and N. Dörfliger (2006), Water storage and transfer in the epikarst of karstic systems during high flow periods, *J. Hydrol.*, *327*, 472–485.

Arfib, B., and G. de Marsily (2004), Modeling the salinity of an inland coastal brackish karstic spring with a conduit-matrix model, *Water Resour. Res.*, *40*, W11506, doi:10.1029/2004WR003147.

Atkinson, T. C. (1977), Diffuse flow and conduit flow in limestone terrain in the Mendip Hills, Somerset (Great Britain), *J. Hydrol.*, *35*(1–2), 93–110.

Bakalowicz, M. (2005), Karst groundwater: A challenge for new resources, *Hydrogeol. J.*, *13*, 148–160.

Bakalowicz, M., P. Crochet, D'D. Hulst, A. Mangin, B. Marsaud, J. Ricard, and R. Rouch (1994), High discharge pumping in a vertical cave: Fundamental and applied results, in *Basic and Applied Hydrogeological Research in French Karst Areas*, edited by M. Bakalowicz and N. Crampon, pp. 93–110, Montpellier-Millau.

Bardot (2001), Cartographie de la galerie noyée des Cent-Fonts, Report n°2001-09, Bardot & Co.

Barenblatt, G. K., I. P. Zheltov, and N. Kochina (1960), Basic concepts in the theory of seepage of homogeneous liquids in fissured rocks, *Prikl. Mat. Mekh.*, *24*(5), 852–864.

Barker, J. A. (1988), A generalized radial flow model for hydraulic tests in fractured rock, *Water Resour. Res.*, *24*(10), 1796–1804.

Bauer, S., R. Liedl, and M. Sauter (2003), Modeling of karst aquifer genesis: Influence of exchange flow, *Water Resour. Res.*, *39*(10), 1285, doi:10.1029/2003WR002218.

Bourdet, D., T. M. Whittle, A. A. Douglas, and Y. M. Pirard (1983), A new set of type curves simplifies well test analysis, *World Oil*, 95–106, May.

de Marsily, G. (1986), *Quantitative Hydrogeology - Groundwater Hydrology for Engineers*, 440 pp., Academic Press, New York.

Debieche, T., Y. Guglielmi, and J. Mudry (2002), Modeling the hydraulical behavior of a fissured-karstic aquifer in exploitation conditions, *J. Hydrol.*, *257*(1–4), 247–255.

Dershovitz, W., P. Wallmann, and S. Kindred (1991), Discrete fracture network modeling for the Stripa characterization and validation drift inflow predictions, SKB Rep. 91-16, Swed. Nucl. Power and Waste Manage. Co., Stockholm.

Ehlig-Economides, C. (1988), Use of the pressure derivative for diagnosing pressure-transient behavior, *J. Pet. Technol*, 1280–1282, Oct.

Ferris, J. G., D. B. Knowless, R. H. Brown, and R. W. Stallman (1962), Theory of aquifer tests. U.S. Geological Survey, Water-Supply Paper 1536E, 174 pp.

Ford, D. C., and P. W. Williams (1989), *Karst Geomorphology and Hydrology*, 601 pp., Academic Division of Unwin Hyman Ltd, London.

Gringarten, A. C., H. J. Ramey Jr., and R. Raghavan (1974), Unsteady-state pressure distributions created by a well with a single infinite conductivity vertical fracture, *Soc. Petrol. Eng. J.*, 347–360, August.

Huang, Y. C., and H. D. Yeh (2007), The use of sensitivity analysis in online aquifer parameter estimation, *J. Hydrol.*, *335*, 406–418.

Jacob, C. E. (1947), Drawdown test to determine effective radius of artesian well, *Trans. Am. Soc. Civ. Eng.*, *112*(2321), 1047–1064.

Jacob, C. E., and S. Lohman (1952), Nonsteady flow to a well of constant drawdown in an extensive aquifer, *Trans. AGU*, *33*(4), 559–569.

Jenkins, D. N., and J. K. Prentice (1982), Theory for aquifer test analysis in fractured rocks under linear (non radial) flow conditions, *Ground Water*, *20*, 12–21.

Jones, W. K. (1999), Pump tests of wells at the National Training Center near Shepherdstown, West Virginia, in: Proceedings of the symposium Karst modeling, *Karst Waters Institute Special Publication*, *5*, 259–261.

Kabala, Z. J. (2001), Sensitivity analysis of a pumping test on a well with wellbore storage and skin, *Adv. Water Res.*, *24*, 483–504.

Kiraly, L. (1984), Régularisation de l'Areuse (Jura Suisse) simulée par modèle mathématique, in *Hydrogeology of Karstic Terraines*, edited by A. Burger and L. Dubertret, pp. 94–99, Heise, Hannover, Germany.

Kruseman, G. P., and N. A. de Ridder (1991), *Analysis and Evaluation of Pumping Test Data*. Publ 47, ILRI, Wageningen.

Ladouche, B., L. Aquilina, E. Petelet, M. Bakalowicz, and R. Schoen (1999), Caractérisation du fonctionnement des systèmes karstiques nord-montpelliérains - Interprétation des données hydrochimiques, *Report R 40940*, 170 pp., BRGM, Montpellier, France.

Ladouche, B., N. Dörfliger, R. Pouget, V. Petit, D. Thiery, and C. Golaz (2002), Caractérisation du fonctionnement des systèmes karstiques nord-montpelliérains - Rapport du programme 1999-2001-Buèges, *Report BRGM/RP-51584-FR*, 200 pp., BRGM, Montpellier, France.

Ladouche, B., J. C. Maréchal, N. Dörfliger, P. Lachassagne, S. Lanini, and P. Le Strat (2005), Pompages d'essai sur le système karstique des Cent-Fonts (Cne de Causse de la Selle, Hérault) - Présentation et interprétation des données recueillies, *Report BRGM/RP 54426-FR*, BRGM, Montpellier, France.

Ladouche, B., J. C. Maréchal, N. Dörfliger, and P. Lachassagne (2006), Système karstique des Cent-Fonts. Simulation de Scénarios d'exploitation et de gestion de la ressource, *Report BRGM/RP-54865-FR*, 269 pp., BRGM, Montpellier, France.

Ladouche, B., J.-C. Maréchal, N. Dörfliger, P. Lachassagne, M. Bakalowicz, I. Valarié, and Ph. Lenoir (2007), Hydrodynamic behaviour during pumping test and modeling of the Cent-Fonts karst system, in *IAH Selected Papers on Hydrogeology*, vol. 10, *Aquifer Systems Management: Darcy's Legacy in a World of Impending Water Shortage*, edited by L. Chery and G. de Marsily, pp. 303–316, Taylor and Francis, United Kingdom.

Liedl, R., M. Sauter, D. Hückinghaus, T. Clemens, and G. Teutsch (2003), Simulation of the development of karst aquifers using a coupled continuum pipe flow model, *Water Resour. Res.*, *39*(3), 1057, doi:10.1029/2001WR001206.

MacQuarrie, K. T. B., and E. A. Sudicky (1996), On the incorporation of drains into three-dimensional variably saturated groundwater flow models, *Water Resour. Res.*, *32*(2), 477–482.

Maillet, E. (1905), *Essais d'hydraulique souterraine et fluviale*, 218 pp., Herman et Cle, Paris.

Maréchal, J. C., B. Dewandel, and K. Subrahmanyam (2004), Use of hydraulic tests at different scales to characterize fracture network properties in the weathered-fractured layer of a hard rock aquifer, *Water Resour. Res.*, *40*, W11508, doi:10.1029/2004WR003137.

Marsaud, B. (1997), A method for interpreting pumping tests in karst aquifers, *Hydrogeologie*, *1997*(3), 31–42.

Mishra, S. (1992), Methods for analyzing single- and multi-well hydraulic test data, in *Grimsel Test Site: Interpretation of Crosshole Hydraulic*

Tests and a Pilot Fluid Logging Test for Selected Boreholes Within the BK Site, edited by S. Vomvoris and B. Frieg, *NAGRA Tech. Rep. NTB 91-09*, Natl. Coop. for the Disposal of Radioactive Waste, Wettingen, Switzerland.

Quinlan, J. F., and R. O. Ewers (1985), Ground water flow in limestone terranes: Strategy rationale and procedure for reliable, efficient monitoring of ground water quality in karst areas, in *Proceedings of the National Symposium and Exposition on Aquifer Restoration and Ground Water Monitoring* (5th, Columbus, Ohio), pp. 197–234, National Water Well Association, Worthington, Ohio.

Ramey, H. J., and A. C. Gringarten (1976), Effect of high-volume vertical fractures on geothermal steam well behavior, in *Proceedings Second U. N. Devel. and Use of Geothermal Resources, San Francisco* vol. 3, pp. 1759–1762, U.S. Government Printing Office, Washington D.C.

Renard, P. (2005), Hydraulics of well and well testing, in *Encyclopedia of Hydrological Sciences*, edited by M. G. Anderson, vol. 3, J. Wiley and Sons, New York.

Reynaud, A., Y. Guglielmi, J. Mudry, and C. Mangan (1999), Hydrochemical approach to the alterations of the recharge of a karst aquifer consecutive to a long pumping period; Example taken from Pinchinade Graben (Mouans-Sartoux, French Riviera), *Ground Water*, *37*(3), 414–417.

Sauter, M. (1992), Quantification and forecasting of regional groundwater flow and transport in a karst aquifer (Gallusquelle, Malm, SW Germany), *Tübinger Geowiss. Arb. C13*, 150 pp., Univ. of Tübingen, Tübingen, Germany.

Streltsova, T. D. (1988), *Well Testing in Heterogeneous Formations*, 413 pp., John Wiley & Sons, New York, NY, United States (USA).

Teutsch, G. (1988), Grundwassermodelle im Karst: Praktische Ansätze am Beispiel zweier Einzugsgebiete im Tiefen und Seichten Malmkarst der Schwäbischen Alb, 205 pp., Ph.D. thesis, Univ. of Tübingen, Tübingen, Germany.

Teutsch, G. (1989), Groundwater models in karstified terrains—Two practical examples from the Swabian Alb, S. Germany, paper presented at 4th Conference on Solving Groundwater Problems with Models, Int. Ground Water Model. Cent., Indianapolis.

Teutsch, G., and M. Sauter (1998), Distributed parameter modeling approaches in karst-hydrological investigations, *Bull. Hydrogéol.*, *16*, 99–109.

Thrailkill, J. (1985), Flow in a limestone aquifer as determined from water tracing and water levels in wells, *J. Hydrol.*, *78*(1–2), 123–136.

Thrailkill, J. (1988), Drawdown interval analysis: a method of determining the parameters of shallow conduit flow carbonate aquifers from pumping tests, *Water Resour. Res.*, *24*(8), 1423–1428.

Vasseur, F. (1993), Exploration dans l'Hérault. Rétrospective historique des plongées souterraines d'exploration dans le département et secteur limitrophes. Les dossiers CELADON, n°3 Aout 1993. Fédération Française de Spéléologie.

Walker, D. D., and R. M. Roberts (2003), Flow dimensions corresponding to hydrogeologic conditions, *Water Resour. Res.*, *39*(12), 1349, doi:10.1029/2002WR001511.

White, W. B. (1969), Conceptual models for carbonate aquifers, *Ground Water*, *7*(3), 15–21.

N. Dörfliger, P. Lachassagne, B. Ladouche, and J.-C. Maréchal, BRGM (Bureau de Recherches Géologiques et Minières), Water Division, 1039 rue de Pinville, 34000 Montpellier, France. (jc.marechal@brgm.fr; jean-christophe.marechal@ird.fr)